International Journal of Chemical and Biochemical Sciences
(ISSN 2226-9614)

Journal Home page: www.iscientific.org/Journal.html

ZnSe films: Properties and applications

Ho Soonmin

[1,*]*Faculty of Health and Life Sciences, INTI International University, 71800, Putra Nilai, Negeri Sembilan, Malaysia.*

Abstract

ZnSe films have been synthesized using different deposition methods, including hydrothermal, RF magnetron sputtering, chemical vapor transport, pulsed laser deposition, the co-precipitation method, and the physical vapor transport method. The prepared films could be used in biomedical labelling devices, field-emitting display devices, light absorbers, window materials, and buffer layers in solar cells. In the morphology investigations, there are several types of results, such as nanorods, nanoclusters, nanosheets, nano-sphere, and nanowires, that could be observed. XRD and TEM results confirmed that heat-treated samples were polycrystalline in nature. Nucleation and growth took place rapidly when the thermal treatment time was increased. The degradation of dye compounds could be observed when exposed to UV light compared to dark conditions.

Keywords: energy efficiency, zinc selenide, thin films, photovoltaic, renewable sources, band gap, energy consumption

*Corresponding Author, e-mail: soonmin.ho@newinti.edu.my

1. Introduction

Nowadays, thin film has emerged as an important technology in the modern world. The properties of the prepared films could be controlled under specific conditions [1-3]. As a result, this material has been used in different applications such as infrared windows [4,5], light-emitting diodes, solar cells [6-8], field emitters, X-ray detectors [9,10], flat panel displays, photodetectors [11,12], sensor devices, biodevices, optoelectronic devices [13,14], electroluminescence, [15,16], and laser devices [17,18]. Solar energy, which is considered clean and renewable energy source, could be used to replace fossil fuels [19-20]. The biggest issue with fossil fuels is releasing carbon dioxide into the environment, causing global warming problems and pollution. Silicon-based solar cells have been developed to generate electricity since a few decades ago [21-23]. However, some limitations were observed, such as space requirements, expensive technology, and weather dependence [24,25]. Therefore, thin film-based solar cells have been designed to replace them. In general, several advantages have been highlighted, such as shorted energy payback, less material consumption [26,27], lighter than silicon-based solar cells, and large-area modules [28,29]. The n-type of zinc selenide is a semiconducting material. It has many properties, including being non-toxic [30,31], high chemical stability, having excellent excitation binding energy, and having a tunable band gap value [32, 33]. In general, structural, thickness, electrical, and physical properties could be controlled via band gap tuning [34,35]. Production of zinc worldwide (from 2005-2022) has been listed [36] in Table 1, while zinc production by country in 2022 has been highlighted [37] in Table 2. The world's largest refinery producer of selenium in 2020 is China, followed by Japan [38], and Russia (Table 3). World demand for selenium in fields such as metallurgy, agriculture, glassmaking, chemical, and pigments. In general, the selenium market is observed to increase, especially in glass manufacturing; however, solar cell applications and metallurgy are expected to decline.

In this work, synthesis and characterization of the prepared zinc selenide films have been reported. Several techniques have been used to study the properties of thin films. Finally, the application of these films has been highlighted.

2. Zinc selenide thin films prepared using various deposition methods

Pulser laser deposition was used to prepare thin films onto quartz substrates (time=30 minutes, laser fluence=0.16 J/cm^2, distance between substrate and target=8 cm). In the FESEM images, it was noticed that a smooth surface was observed in the as-deposited films. Nucleation and growth took place rapidly when the thermal treatment time was increased. As a result, larger particles with well-developed nanorods were produced. Figure 1 shows nanorods (length=15 μm, diameter=200 nm) covered the surface of the

substrate completely [39] and displayed a high surface-to-volume ratio, which can improve photodegradation for the films prepared when the thermal treatment time was 12 hours. The obtained experimental results indicated that optical transmission was reduced but the density of nanorods increased when the treatment time was increased. Higher photocatalytic degradation of the methyl orange dyes could be seen in nanorods (60%) if compared to ZnSe films (18%), exposure to UV light, and 180 minutes. ZnSe-based detectors [40] have been prepared using a zinc selenide substrate (thickness of 1 mm) doped with aluminum (concentration of $10^{18}cm^{-3}$), nickel layer (10 nm =thickness) and the indium layer (100 nm=thickness) acted as Schottky barriers and ohmic contact, respectively (Figure 2). The obtained detectors showed excellent responsivity (UV-A=50 mA/W, UV-B=10 mA/W) and low dark current. The speed and responsivity of the unfiltered detectors were observed to be 300 kHz, and 110 mA/W, respectively. In the current-voltage studies, low-leakage current (20 nA) could be detected when the reverse bias was 0.5V. Obviously, leakage current increases quickly (at +0.4V), because of diode breakdown.

RF magnetron sputtering was utilized to synthesize films on glass substrates (temperature=220 °C, distance between substrate and target=8 cm, sputtering time=30 minutes). Electron mobility, band gap (2.56 eV to 2.64 eV), crystallite size (51.8 nm -107.4 nm), and thickness (37nm-351 nm), narrowness of (111) peak increased, but root mean square roughness and average roughness decreased when the RF power was increased from 60 W to 120 W. Au/ZnSe/Au structures were made at 300 K as highlighted in the current-voltage dark investigations (figure 3), indicating nonlinear but symmetrical properties [41]. The optimized plasma power was 100 W, showing a flat surface, the smallest roughness value, better crystallinity, and excellent electrical properties. Obviously, the prepared films could be used as light absorbers, window materials, and buffer layers in solar cells. Technically speaking, loss of proton was achieved via the doping process, which is accountable for charge carriers in photocurrents. The influence of foreign particles on zinc selenide was studied using a genetic algorithm in the support vector regression algorithm. The band gap is reduced (figure 4) after adding copper-indium [42] and sulfur, which by moving the absorption edge to a longer wavelength region, could improve the photo absorption process. On the other hand, nickel doped zinc selenide film [43] has been produced using the hydrothermal method (precursors=zinc chloride, sodium selenite, reducing agent=hydrazine hydrate, temperature=180 °C). According to XRD analysis, the diffraction peaks moved towards higher angles (from 27.252° to 27.48°), indicating Ni^{2+} ions have occupied Zn^{2+} ion sites. Experimental findings confirmed that crystallite size (11 nm to 8 nm), lattice constant (5.658 to 5.63) decrease, but dislocation density (8.26 to 15.62 $x10^{15}$ line/m^2), band gap (2.47 eV to 2.8 eV), strain value (0.138 to 0.2513) and emission peak intensity (photoluminescence spectra) increase when the nickel concentration is increased. According to high-resolution transmission electron microscopy (HRTEM) studies, agglomerated spherical nanoparticles and a homogeneous surface could be seen. The size distribution was found to be 10-35 nm and 10-20 nm in pure samples and doped films, respectively. SEM images confirmed that Ostwald ripening causes the formation of nanospheres, while a selective area diffraction pattern revealed that polycrystalline is in nature. Behnaz and co-workers [44] have reported that zinc selenide was doped with rare earth elements through a chemical vapor transport technique. Lower band gap energy (figure 5) in ZnSe-Eu (2.201eV-2.250 eV) and ZnSe-Eu-Yb (2.562 eV to 2.492 eV) if compared to pure zinc selenide (2.67 eV). In the photoluminescence (PL) spectra, band A (637 nm) and B (610 nm) could be identified at a lower temperature in the pure sample than ZnSe-Eu (250 K). It was noticed that more narrow emission peaks could be seen in the ZnSe-Eu-Yb sample. Experimental findings confirmed that these samples emit light in the near infrared and visible range and can be used in optoelectronic devices, LED, and diode lasers. The zincblende phase of films was prepared using the mechanical milling method [45] and hydrothermal technique. Based on the Raman spectroscopy, several modes, such as 2TA (138 cm^{-1}), TO (201 cm^{-1}), LO (247 cm^{-1}) and 2LO (492 cm^{-1}) could be identified as zincblende structures. Obviously, the peak intensities decreased, and the peak position moved to a lower frequency with increasing milling time. The TEM image highlighted a sphere shape with an average size of 20-100 nm. There are two peaks (462 nm and 520-555nm) could be seen in photoluminescence analysis. All the results demonstrated that removal efficiency was less than 20% in dark conditions for 30 minutes. It is evident that rapid photocatalytic degradation occurred (30%) at the very beginning (about 15 minutes) and reached 80% after 150 minutes in the presence of UV-light conditions when the milling time was 60 minutes. The Rhodamine B decomposition using zinc selenide nanoparticle has been explained, and the final products were expected to be carbon dioxide and water (figure 6). Zinc selenide absorbs ultraviolet light to produce electron and hole pairs. The hole pairs were trapped on the surface of the nanoparticle and formed reactive hydroxyl radicals. Oxygen reacted with electrons to generate superoxide anion radicals and combined with protons to produce HO_2. Zinc blende phase (diameter=80 nm, average length=2-3 μm) and smooth surface were observed in manganese (Mn) doped zinc selenide films. There are two emission bands (432 nm and 540 nm) that appeared in the PL spectrum [46]. The selected area electron diffraction (figure 7) revealed a single well-crystallized, along (200) direction. An interesting pattern could be observed in UV-visible absorption spectra. The band gap could not be reduced when the concentration of manganese was 5%. However, manganese was unable to enter the internal lattice if its concentration was very high (20 %). In this case, the best concentration was 10 % and showed a sharp absorption peak at 360 nm. Researchers have pointed out that these nanowire materials could be employed for biomedical labelling reagents. Comparative analysis (Table 4) of films growing onto different substrates through the chemical vapor deposition method has been reported [47]. Indium tin oxide (ITO) glass is employed as a transparent electrode, but it has some disadvantages (very poor flexibility, and very limited quantities). Graphene is defined as a two-dimensional material and has many advantages (flexibility, high electron mobility, conductivity, and transparency). Silicon dioxide (SiO2) is an amorphous material widely utilized due to several factors such as biocompatibility, stability, and ease of preparation. In the FESEM analysis, the average diameter was 20-60 nm and the length was more than 5 μm in all samples.

Table 1: Production of zinc globally (2005-2022) [36].

Year	Zinc production (thousand tons)
2005	10128
2006	10431
2007	11203
2008	11882
2009	11601
2010	12347
2011	12585
2012	12892
2013	13039
2014	13418
2015	13622
2016	12668
2017	12683
2018	12723
2019	12799
2020	12252
2021	12801
2022	12483

Table 2: Worldwide zinc production (by country) in 2022 [37].

Country	(thousand tons)
China	4200
Peru	1400
Australia	1300
India	830
United States	770
Mexico	740
Bolivia	520
Russia	280
Sweden	250
Canada	250

Table 3: Global refinery production selenium in 2020 [38]

Country	production (thousand tons)
Belgium	200
Canada	60
China	1200
Finland	84
Germany	300
India	14
Japan	740
Peru	35
Poland	74
Russia	340
Sweden	10
Turkey	50
Serbia	10

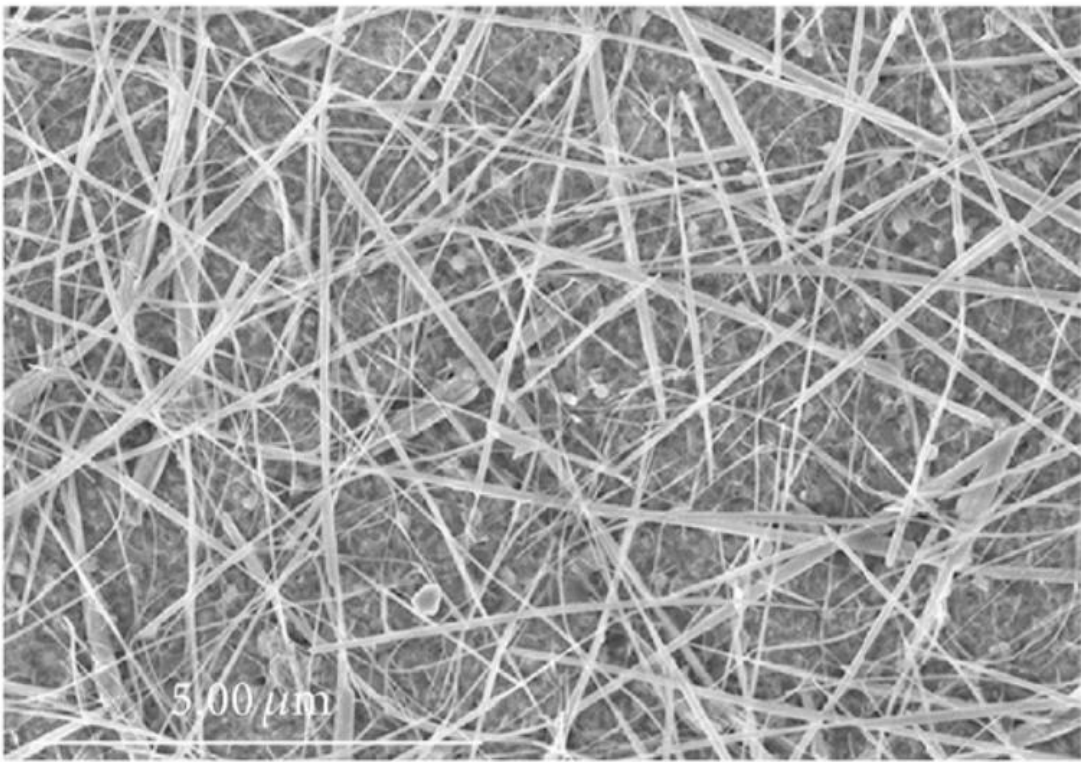

Figure 1: FESEM image of pulse laser-deposited ZnSe films [39]

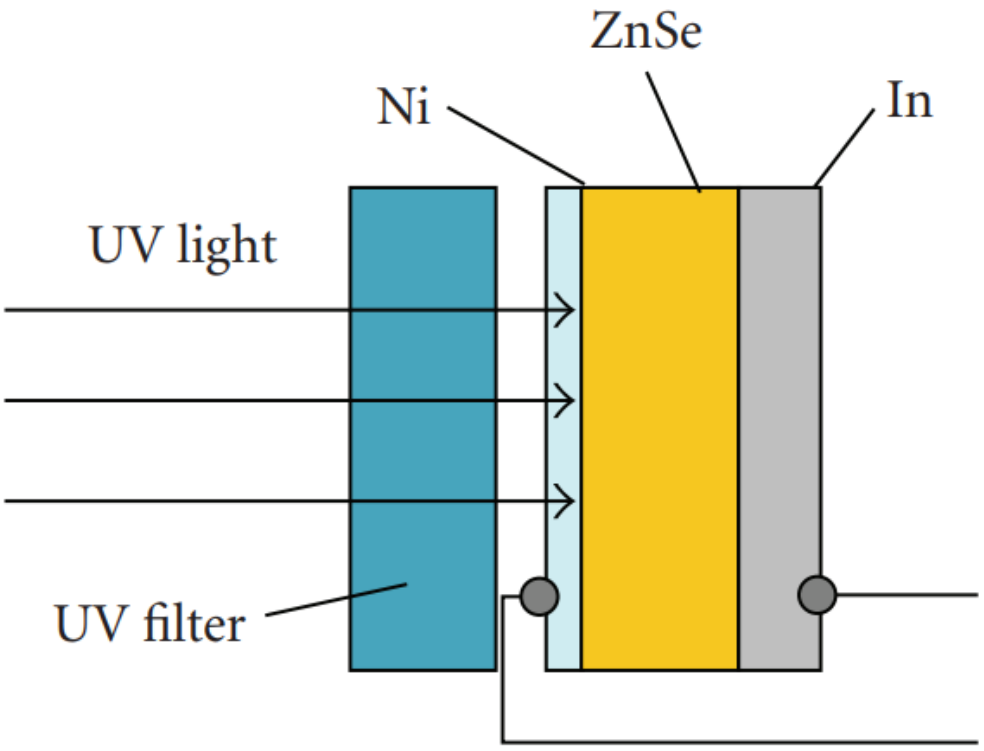

Figure 2: Schematic diagram of the Schottky diode [40]

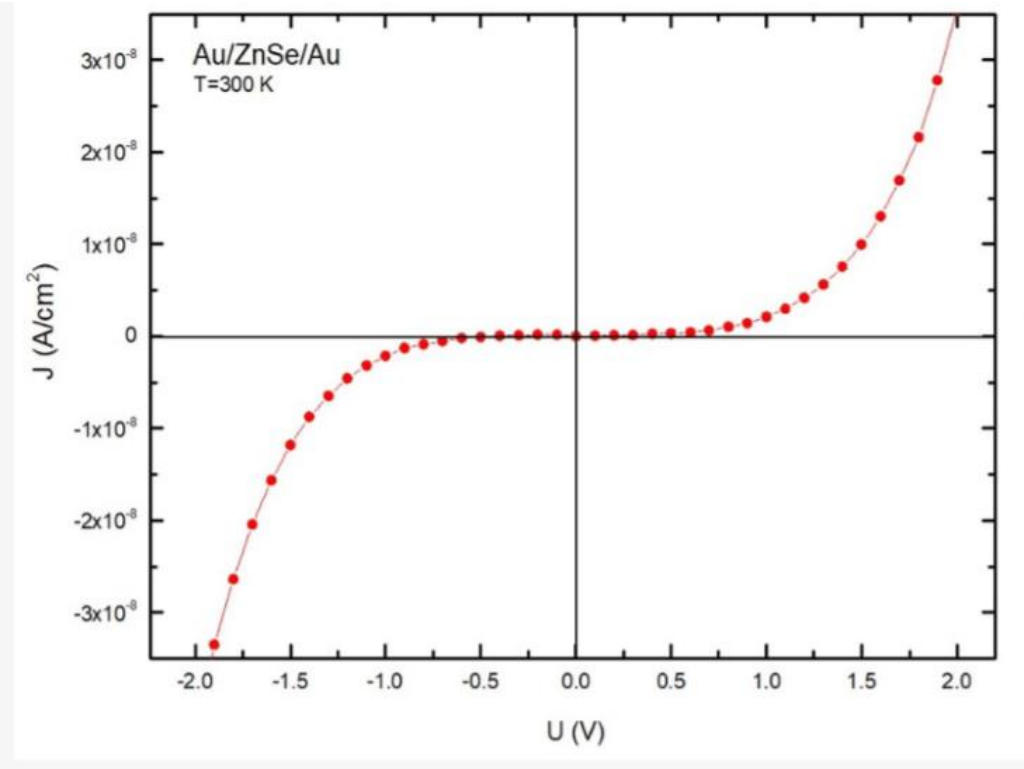

Figure 3: Current-voltage dark characteristics of sputtered ZnSe films [41]

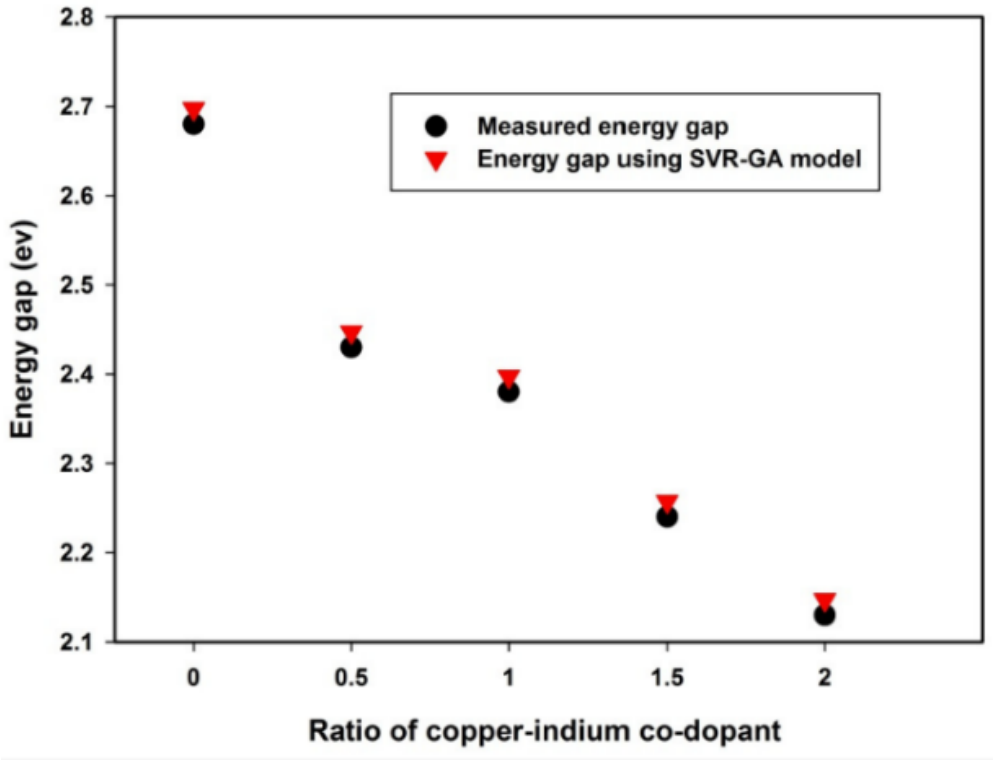

Figure 4: The influence of ratio of copper-indium on the band gap [42]

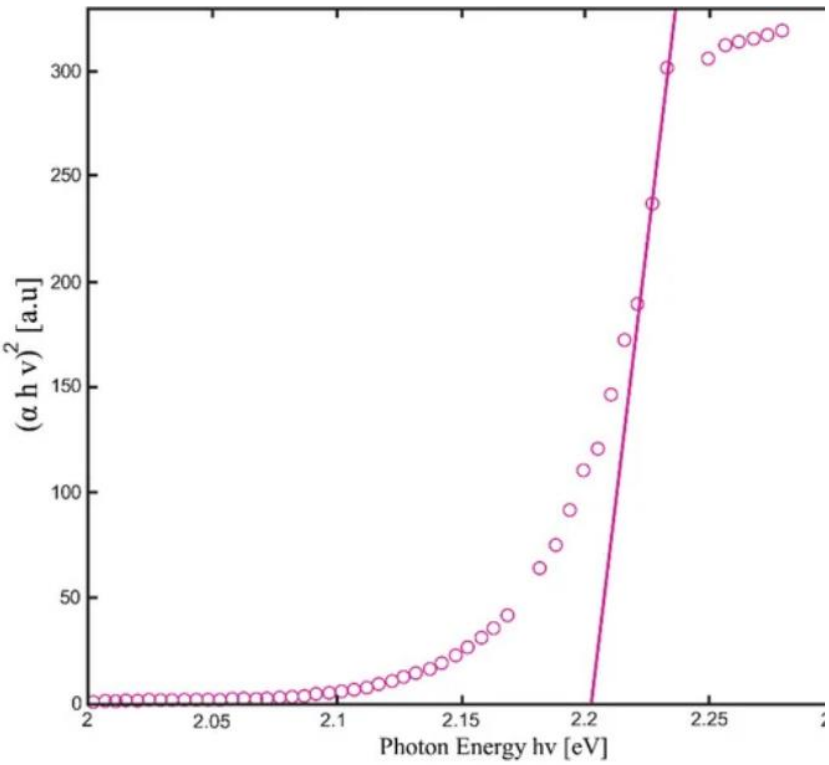

Figure 5: Energy gap measurement for ZnSe:Eu^{3+} thin films at 300 K [44]

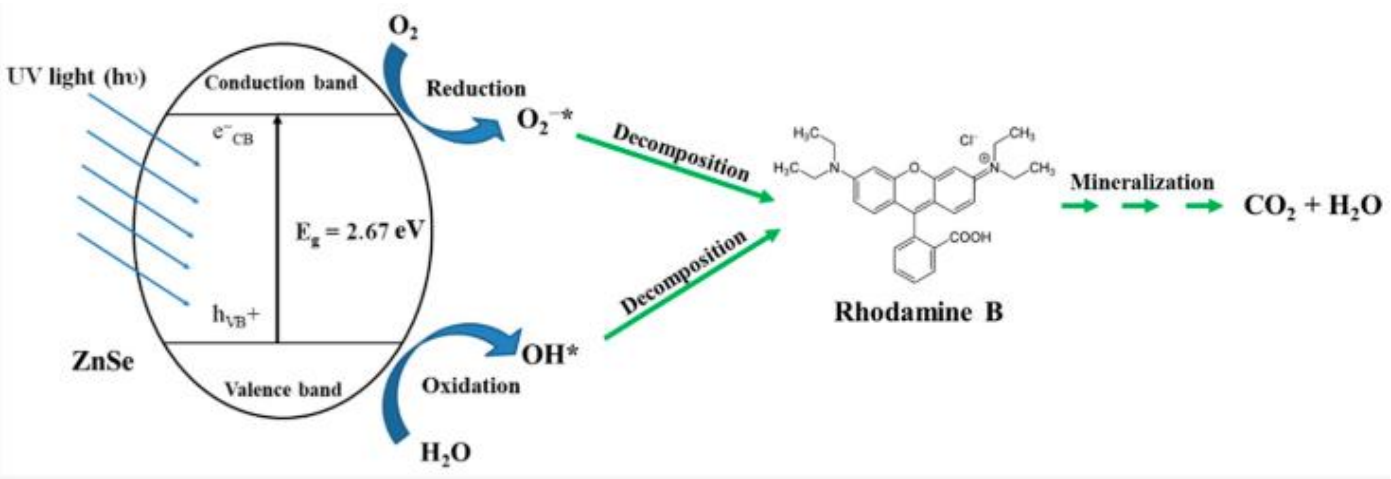

Figure 6: Rhodamine B decomposition using zinc selenide nanoparticles [45].

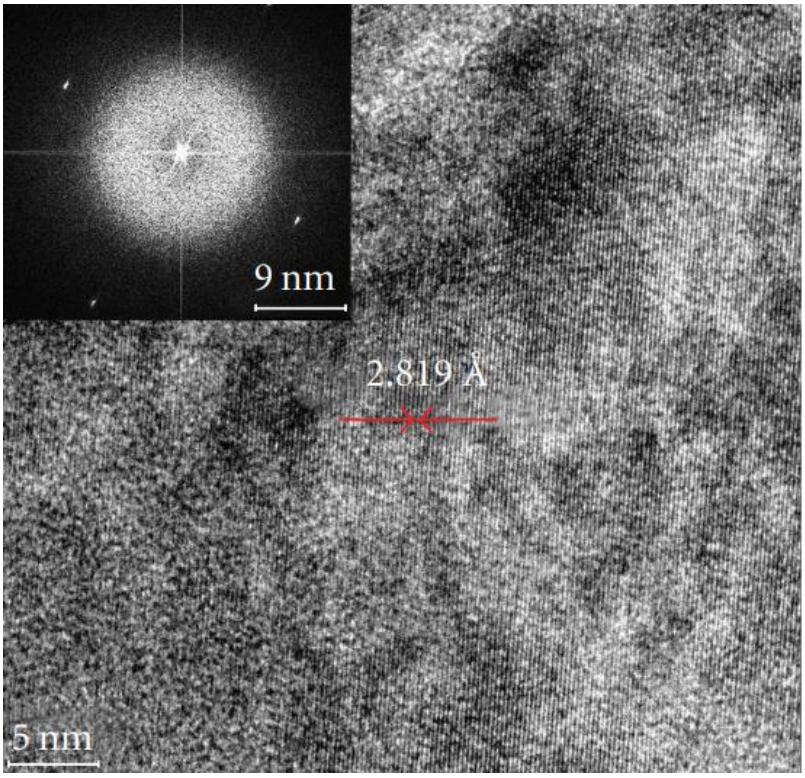

Figure 7: Selected area electron diffraction image of the Mn-doped ZnSe nanowires [46].

Table 4: Properties of the zinc selenide films prepared using different types of substrates.

	ITO glass	SiO_2 glass	Graphene
Structure properties	Cubic and hexagonal	Cubic	Cubic
Illumination properties	Reddish-orange	Not luminescent	Reddish-orange
HRTEM	Growth direction of (100) and (200)	Growth direction of (111)	Growth direction of (111)
PL	1.977 eV (627 nm)	2.701 eV (459 nm)	1.977 eV (627 nm), 2.695 eV (460 nm)

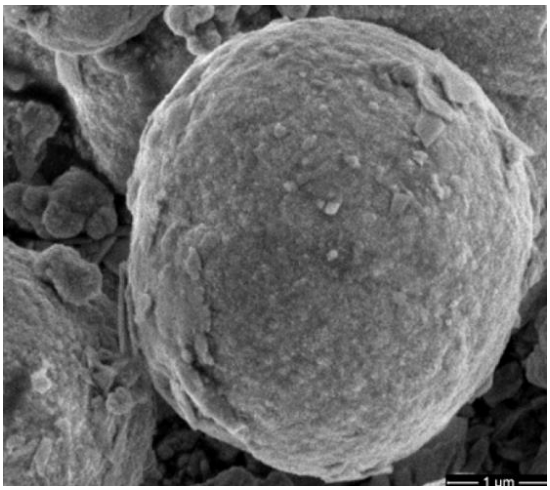

Figure 8: SEM image of zinc selenide films. [50]

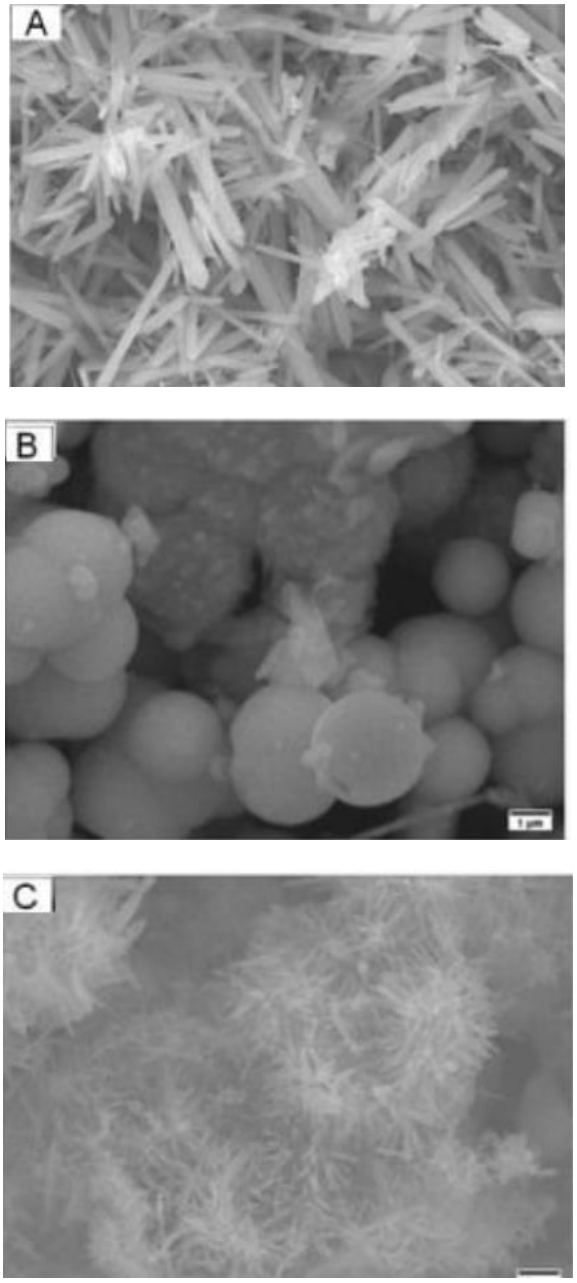

Figure 9. SEM images of nanorods (**A**), nanospheres (B) and nanoclusters (C) [51]

Table 5: Several types of thin films have been used for antibacterial activities.

Thin films	Results	Researchers
CdS	CdS/natural aluminosiloicate nanotubes indicated 100% E Coli growth inhibition when the concentration was 1000 μg/mL, under visible light [52]. CdS/MCM-41/HNT and CdS/SBA15 indicated bacteriostatic effects at concentrations of 63 μg/mL.	Anna and co-workers, 2022
CdSe	The inhibition zone was observed to be higher for *Bacillus subtilis* and *Staphylococcus aureus* when using 0.001 wt% CdSe quantum dots (prepared using the hot injection method). Antibacterial activity index [53] was detected to be 83.3, 52.2, 50, and 82.6 for *Staphylococcus aureus, Bacillus subtilis, Escherichia coli,* and *Pseudomonas aeruginosa, respectively.*	Meikhail and co-workers, 2018
ZnS	Inhibition zone increased (17.5 mm to 21 mm), when the concentration of zinc sulfide was increased from 20 mg/mL to 40 mg/mL for E. Coli, and from 14 mm to 21 mm for S. *aureus* strains, respectively [54]. ZnS exhibited antimicrobial activity for *K. pneumoniae (14 mm), Bacillus* sp. (10.4 mm) and *S. saprophyticus* (16 mm) when the concentration of ZnS was 40 mg/mL.	Aileen and co-workers, 2023
CuS	CuS-BSA showed slight toxicity (50 μg/mL) to *B. subtilis* after 3 min, under illumination conditions (0.7 W cm^{-2}). Copper sulfide nanoparticles are non-toxic to bacteria at room temperature (at 200 μg/mL). A reduction in bacterial growth could be observed when the lysozyme is released under NIR-light illumination [55]. The bacterial strain (*B. subtilis*) could be destroyed completely under illumination of 0.7 W/cm using CuS-BSA/lysozyme at 200 μg/mL.	Abir and co-workers, 2021
CuS	Copper sulfide thin films have been prepared via hydrothermal process using copper nitrate and thiourea [56]. Copper sulfide nanoparticles are smaller in size and therefore display higher antibacterial efficiency (E Coli) than nanosheets. Electron spin resonance spectroscopy showed that all types of copper sulfide films generated hydroxyl and superoxide radicals under simulated solar light irradiation. Reactive oxygen species generation will be significantly increased in nanosheets (4.6 folds) and nanoparticles (3.5 folds), respectively. Bacterial cell walls will be destroyed in nanoparticles and nanosheets under NIR laser.	Mutalik and co-workers, 2022
Cu-doped ZnS, Al-doped ZnS	These materials have been prepared onto glass substrates through the sol-gel dip coating method. Higher zone of inhibition for gram-negative bacteria (E. Coli and P. Aeruginosa) because of the smaller crystallite size and larger surface area [57]. At a concentration of 60 μg/mL, the highest inhibition zone was observed to be 11 mm, 11 mm, 10 mm, 9 mm, 9 mm and 6 mm for E. coli, A. niger, C.albicans, P.aeruginosa, S.aureus, and B.subtilis using 2% copper doped zinc sulfide films. At the concentration of 60 μg/mL, the highest zone of inhibition was found to be 9 mm, 10 mm, 10 mm, 10 mm, 9 mm, and 8 mm for P.aeruginosa, S.aureus, A. niger, C.albicans, E.coli,and B.subtilis using 2 % aluminium doped zinc sulfide.	Saroja and co-workers, 2019
ZnS	This is well reported that the inhibition zone increases when the concentration of ZnS is increased. FTIR results have confirmed the complexation between zinc sulfide nanoparticles and polymer blends [58].	Menna and co-workers, 2021

It is proven that field-emitting display devices could be produced using zinc selenide films deposited onto graphene. The obtained devices indicated red emission with Commission International de L'Eclairage coordinates of (0.621, 0.315). Physical vapor transport method has been used to prepare sulfur, chromium, and iron doped zinc selenide films [48]. The composition was $Zn_{0.96}Fe_{0.04}Se$ and the iron concentration was very low ($4.6x10^{-4}$ ppm). Researchers have highlighted that did not see gross defects on the polished surface. However, small cracks could be seen on the edge of the slab. Based on the SEM studies, we can see microfacets and grain boundaries throughout the crystals because of the high thermal gradient. In addition, there were no microvoids and overgrown crystallites in the obtained samples because of the very low iron concentration. Prepared samples could be utilized for tuning devices because the dielectric constant has been tuned successfully as a function of frequency. Chromium doped films show a composition of $Zn_{0.987}Cr_{0.013}Se$ and the concentration of chromium was $3.2x10^{-3}$ ppm. Experimental results show that this sample is reddish and did not show any cracks in the slabs. SEM images confirmed that there were big, faceted microplates with no uniform structure (thickness=0.5 μm, length=5 μm). Resistivity and dielectric constant decrease as a function of frequency; a lower dielectric constant could also be observed if compared to other samples. However, it had a higher resistivity value (three times) than other samples because chromium was a deep-level dopant. Sulfur doped samples showed a composition of $ZnSe_{0.91}S_{0.09}$. Based on XRD studies, a sharp peak at the (111) plane could be seen, and the diffraction peak was moved to higher angles than pure zinc selenide. According to SEM analysis, small microvoids have been identified because of the changes in deposition rates. Resistivity and dielectric constant values decrease with frequency (100 kHz-100000kHz). However, these values were higher than those of pure zinc selenide powder.

Strontium doped zinc selenide has been synthesized [49] through the co-precipitation method (reducing agent=sodium borohydride, stabilizing agent=2-mercaptoethanol). In structural studies, crystallite size is 12 nm in a pure sample; however, crystallite size increases when the molar ratios of strontium are increased from 0.01 (21 nm), 0.05 (26 nm) to 0.1 (35 nm). The characteristic peaks of 1575 cm-1, 1359 cm-1, 1249 cm-1 and 1021 cm-1 denote the formation of OH bending, CO stretching and CH bending, respectively, using a low concentration of strontium. In addition, these peaks will move towards the lower wavelength region when the concentration of strontium is increased. In the Ultraviolet (UV)-Diffuse reflection spectroscopy (DRS) investigations, the absorption peak appeared in the visible and UV regions for Sr-doped samples and pure zinc selenide films, respectively, because of the transition of electrons in Zn2p and Se 3d. In the morphology studies, different results could be observed at low (nanosheets) and higher concentrations (nanoflower with a larger surface area) of dopant. In the chemical composition studies, it was demonstrated that zinc ($Zn\ 2p_{1/2}$=1022.5 eV, $Zn2p_{3/2}$=1045.46eV), selenium ($Se\ 3d_{5/2}$=55.34 eV, $Se\ 3d_{3/2}$=59.01 eV) and strontium atom (Sr-3d=134.93 eV) binding energies have been identified in the XPS spectra. In the antibacterial activity, Staphylococcus aureus (0.5 mm to 5 mm) and Escherichia coli (0.8 mm to 5.1 mm) were used and showed excellent biological activity when the concentration of Sr-doped zinc selenide was in the range of 25 μL to 100 μL. In the photocatalytic methyl orang dye degradation process, dye degradation was 75% in the pure sample; however, the percentage of degradation increased (79%, 81% to 88%) when the molar ratios were increased due to improved electronic properties.

The hydrothermal technique [50] has been used to prepare micrometre-sized sphere (figure 8) of zinc selenide thin films in the presence of sodium selenite and zinc sulphate (time=3 hours, temperature=140 °C). Based on the UV-visible spectroscopy, this sample shows a broad absorption band at 400-600 nm. The growth of *Staphylococcus aureus* was inhibited after 4 hours, and this material proves to be active against *S. aureus*, the survival cell percentage was 7.6%. Further analysis revealed that a 100% reduction was observed under visible light for 10 minutes. On the other hand, analyzing the data confirmed that the number of *Micrococcus Iysodeikticus* cells reduced significantly, and the bacterial reduction achieved 94.13%.

Penicillium and Aspergillus species can produce toxins such as Ochratoxin A (molar mass of 403.813 g/mol and chemical formula of $C_{20}H_{18}ClNO_6$). It causes carcinogenic, mutagenic, immunotoxin, and teratogenic. Nanorods (average width=150 nm to 260 nm), nanoclusters (average size=75 nm to 260 nm) and μ-spheres (average size=1100 nm to 2400 nm) of films have been prepared through microwave-assisted hydrothermal technique [51] and the morphology study (figure 9) was conducted through scanning electron microscopy (SEM) technique. In the fluorescence analysis, the highest quenching efficiency was found in μ-spheres due to their larger size and highly negative surface charge. Also, it was proven that μ-spheres show very strong interaction with Rhodamine B dye compounds because they are stable, highly dispersive, and negatively charged. Detection of ochratoxin A is carried out using μ-spheres-based zinc selenide fluorescent aptasensor, low detection limit was 0.07 ng/L (linear range of 0.1 to 200 ng/L). Based on the literature survey (Table 5), there are several types of thin films that have been used in antibacterial activities for gram-negative bacteria and gram-positive bacteria. Zone of inhibition and antibacterial efficiency were studied using CdS, CdSe, ZnS, CuS, Cu-doped ZnS, and Al-doped ZnS.

3. Conclusions

Several deposition techniques, such as hydrothermal, RF magnetron sputtering, chemical vapor transport, pulsed laser deposition, the co-precipitation method, and physical vapor transport method, have been used to prepare zinc selenide thin films. The prepared films show different morphologies, including nanorods, nanoclusters, nanosheets, nano-spheres and nanowires. Structural studies revealed that polycrystalline in nature could be observed in heat-treated samples, as highlighted by TEM and XRD analysis. Nucleation and growth took place rapidly when the thermal treatment time was increased. The degradation of dye compounds could be observed when exposed to UV light compared to dark conditions. A zone of inhibition test was conducted for gram-negative bacteria and gram-positive bacteria. Experimental results indicated that antibacterial

activities were strongly dependent on experimental conditions.

Acknowledgements:

Author would like to thank INTI International University, Malaysia for the financial support.

References

[1] T. Sinha, D. Lilhare and A. Khare. (2019). A review on the improvement in performance of CdTe/CdS thin-film solar cells through optimization of structural parameters. Journal of Materials Science. 54: 12189–12205.

[2] T. Zian, S. Tan and N. Yusoff. (2022). Development of polarization modulator using Mxene thin film. Scientific Reports. doi: 10.1038/s41598-022-10768-x.

[3] A. Ojo and M. Dharmadasa. (2017). Analysis of electrodeposited CdTe thin films grown using cadmium chloride precursor for applications in solar cells. Journal of Materials Science: Materials in Electronics. 28: 14110–14120.

[4] L. Xu, S. Guo and V. Ralchenko. (2023). Progress in infrared transparencies under opto electro thermo and mechanical environments. Surface Science and Technology. https://doi.org/10.1007/s44251-023-00002-9.

[5] P. Li, N. Wang and X. Che. (2013). Infrared transmissive and rain-erosion resistant performances of GeC/GaP double-layer thin films on ZnS substrates. Applied Surface Science. 264: 538–544.

[6] S.M. Ho. (2022). A review of metal oxide thin films in solar cell applications. International Journal of Thin Film Science and Technology. 11: 37-45.

[7] K. Park, J. Park and S. Park. (2017). Fabrication of Cd-free $CuInSe_2$ solar cells using wet processes. Journal of Materials Science. 52: 13533–13540.

[8] N. Saravanan, K. Anuar and S.M. Ho. (2010). Effect of deposition time on surface topography of chemical bath deposited PbSe thin films observed by atomic force microscopy. Pacific Journal of Science and Technology. 11: 399-403.

[9] M. Dharmadasa and A. Ojo. (2017). Unravelling complex nature of CdS/CdTe based thin film solar cells. Journal of Materials Science: Materials in Electronics. 28: 16598–16617.

[10] K. Kim, K. Cha and S. Jeon. (2014). Photo-responsivity characterizations of CdTe films for direct-conversion X-ray detectors. Journal of the Korean Physical Society. 65: 446–449.

[11] Z. Aba, A. Goktas and A. Kilic. (2023). Characterization of $Zn_{1-x}La_xS$ thin films; compositional, surface, optical, and photoluminescence properties for possible optoelectronic and photocatalytic applications. Journal of Sol-Gel Science and Technology. https://doi.org/10.1007/s10971-023-06273-w.

[12] Y. Liu, Z. Li and W. Zhong. (2014). Synthesis and photoluminescence properties of ZnS nanobowl arrays via colloidal monolayer template. Nanoscale Research Letters. https://doi.org/10.1186/1556-276X-9-389.

[13] N. Gopakumar, S. Anjana and K. Vidyadharan. (2010). Chemical bath deposition and characterization of CdSe thin films for optoelectronic applications. Journal of Materials Science. 45: 6653–6656.

[14] S. Yılmaz, I. Polat and M. Tomakin. (2020). Transparent and conductive CdS:Ca thin films for optoelectronic applications. Applied Physics A. https://doi.org/10.1007/s00339-020-03752-7.

[15] M. Hayashi, N. Sugimoto and S. Fujiwara. (1998). Electroluminescence from CdSe microcrystals-doped indium tin oxide thin films. Journal of Materials Science. 33: 4829–4833.

[16] B. Dabbousi, O. Onitsuka and M. Rubner. (1994). Size Dependent Electroluminescence from CdSe Nanocrystallites (Quantum Dots). MRS Online Proceedings Library. https://doi.org/10.1557/PROC-358-707.

[17] B. Ullrich. (2007). Thin-film CdS formed with pulsed-laser deposition towards optical and hybrid device applications. Journal of Materials Science: Materials in Electronics. 18: 1105–1108.

[18] E. Shaffer, S. Helmy and D. Drouin. (2008). Excimer laser-induced crystallization of CdSe thin films. Applied Physics A. 93: 869–874.

[19] C. Li, X. Fan and Y. Wang. (2023). Can the development of renewable energy in China compensate for the damage caused by environmental pollution to residents' health? Environmental Science and Pollution Research. 30: 92636–92650.

[20] P. Huang and Y. Liu. (2017). Renewable Energy Development in China: Spatial Clustering and Socio-Spatial Embeddedness. Current Sustainable Renewable Energy Reports. 4: 38–43.

[21] Y. Lee, B. Kim and M. Ifitiquar. (2014). Silicon solar cells: Past, present and the future. Journal of the Korean Physical Society. 65: 355–361.

[22] H. Martin, S. Glunz and C. Jan. (2020). Passivating contacts and tandem concepts: Approaches for the highest silicon-based solar cell efficiencies. Applied Physics Reviews. https://doi.org/10.1063/1.5139202.

[23] B. Rech, S. Calnan and T. Kilper. (2006). Challenges in microcrystalline silicon based solar cell technology. Thin Solid Films. 511-512: 548-555.

[24] I. Yukimi, Y. Takashi and T. Hama. (2001). Production technology for amorphous silicon-based flexible solar cells. Solar Energy Materials and Solar Cells. 66: 107-115.

[25] C. Lucio, K. Piotr and R. Lisa. (2019). Silicon solar cells: toward the efficiency limits. Advances in Physics: X, https://doi.org/10.1080/23746149.2018.1548305.

[26] P. Zaretskaya, V. Gremenyuk and V. Zalesskii. (2000). The properties of $CuInSe_2$ films obtained by

selenation of Cu-In layers. Technical Physics. 45: 1371–1373.

[27] K. Anuar, S.M. Ho and N. Saravanan. (2010). The effect of bath temperature on the chemical bath deposition of copper sulphide thin films. Jordan Journal of Chemistry. 5: 165-173.

[28] M. Sadigov, M. Özkan and E. Bacaksiz. (1999). Production of $CuInSe_2$ thin films by a sequential processes of evaporations and selenization. Journal of Materials Science. 34: 4579–4584.

[29] S.M. Ho, M. Bilal and R. Das. (2019). Preparation of thin films by SILAR and spin coating method. Eurasian Journal of Analytical Chemistry. 14: 165-172.

[30] D. Jeroh, A. Ekpunobi and D. Okoli. (2023). Growth of nanostructured zinc selenide films doped with europium and their possible applications. Applied Nanoscience. 13: 4605–4611.

[31] B. Mohammad, R. Mahmoudian and A. Nejad. (2021). Fabrication of ZnSe Thin Solid Films on the Cu Substrate and Investigation of Electrochemical, Adhesion and Solar Cell Properties by a New Technique. Russian Journal of Electrochemistry. 57: 567–579.

[32] A. Dawar, P. Shishodia and P. Mathur. (1989). Growth of zinc selenide thin films. Journal of Materials Science Letters. 8: 561–562.

[33] H. Yudar, S. Pat and S. Korkmaz. (2017). Zn/ZnSe thin films deposition by RF magnetron sputtering. Journal of Materials Science: materials in electronics. 28: 2833–2837.

[34] J. Sharma, D. Shikha and S. Tripathi. (2012). Electrical characterization of nanocrystalline zinc selenide thin films. Journal of Theoretical and Applied Physics. https://doi.org/10.1186/2251-7235-6-16.

[35] A. Khomchenko. (1997). Structure and nonlinear optical properties of zinc selenide films. Techical Reports. 42: 1038–1040.

[36] https://www.statista.com/statistics/264882/world-mine-production-of-zinc/

[37] https://www.statista.com/statistics/264634/zinc-production-by-country/

[38] https://pubs.usgs.gov/periodicals/mcs2022/mcs2022-selenium.pdf

[39] Y. Jiajia, Y. Chao and S. Zhou. (2016). Fabrication and Photocatalytic Properties of ZnSe Nanorod Films. Journal of Nanomaterials. http://dx.doi.org/10.1155/2016/1738608.

[40] V. Naval, C. Smith and F. Alves. (2010). Zinc Selenide-Based Schottky Barrier Detectors for Ultraviolet-A and Ultraviolet-B Detection. Advances in OptoElectronics. doi:10.1155/2010/619571.

[41] T. Ovidiu, A. Radu and L. Ion. (2021). Effect of RF Power on the Physical Properties of Sputtered ZnSe Nanostructured Thin Films for Photovoltaic Applications. Nanomaterials. https://doi.org/10.3390/nano11112841.

[42] O. Olusayo, B. Latif and O. Taoreed. (2022). Tailoring the Energy Harvesting Capacity of Zinc Selenide Semiconductor Nanomaterial through Optical Band Gap Modeling Using Genetically Optimized Intelligent Method. Crystals. https://doi.org/10.3390/cryst12010036.

[43] R. Divya, G. Vinitha and N. Manikandan. (2019). Synthesis and characterization of nickel doped zinc selenide nanospheres for nonlinear optical applications. Journal of Alloys and Compounds. 791, 601-612.

[44] A. Behnaz, H. Khalid and M. Nawal. (2022). On the Absorption and Photoluminescence Properties of Pure ZnSe and Co-Doped ZnSe:Eu^{3+}/Yb^{3+} Crystals. Applied Sciences. https://doi.org/10.3390/app12094248.

[45] H. Bui, K. Chi and V. Mai. (2021). Structural, Optical, and Photocatalytic Properties of ZnSe Nanoparticles Influenced by the Milling Time. Crystals. https://doi.org/10.3390/cryst11091125.

[46] D. Han, C. Song and X. Li. (2010). Synthesis and fluorescence property of Mn-doped ZnSe nanowires. Journal of Nanomaterials. https://doi.org/10.1155/2010/290763.

[47] K. Seo, H. Shin and J. Kim. (2015). Substrate-Dependent Differences in the Crystal Structures and Optical Properties of ZnSe Nanowires. Journal of Nanomaterials. http://dx.doi.org/10.1155/2015/201420.

[48] S. Bahadur, P. Gill and C. Su. (2020). Effect of Doping on the Electrical Characteristics of ZnSe. Crystals. https://doi.org/10.3390/cryst10070551.

[49] V. Beena, S. Rayar and A. Awais. (2021). Synthesis and Characterization of Sr-Doped ZnSe Nanoparticles for Catalytic and Biological Activities. Water. https://doi.org/10.3390/w13162189.

[50] A. Crina, M. Jose and M. Enache. (2023). Antibacterial Activity of ZnSe, ZnSe-TiO_2 and TiO_2 Particles Tailored by Lysozyme Loading and Visible Light Irradiation. Antioxidants. https://doi.org/10.3390/antiox12030691.

[51] M. Azhar, A. Hayat and M. Fazal. (2022). Multifunctional Smart ZnSe-Nanostructure-Based Fluorescent Aptasensor for the Detection of Ochratoxin A. Biosensors. https://doi.org/10.3390/bios12100844.

[52] S. Anna, C. Kirill and S. Eliza. (2022). Photoinduced Antibacterial Activity and Cytotoxicity of CdS Stabilized on Mesoporous Aluminosilicates and Silicates. Pharmaceutics. 10.3390/pharmaceutics14071309.

[53] M. Meikhail, M. Awad and A. Abdelghany. (2018). Role of CdSe quantum dots in the structure and antibacterial activity of chitosan/poly-ε-caprolactone thin films. Egyptian Journal of Basic and Applied Sciences. 5: 138-144.

[54] S. Aileen, P. Hector and B. Noelia. (2023). Sulfidogenic Bioreactor-Mediated Formation of ZnS Nanoparticles with Antimicrobial and Photocatalytic Activity. Nanomaterials (Basel). doi: 10.3390/nano13050935.

[55] S. Abir, G. Sena and A. Ahmed. (2021). Enhanced Antibacterial Activity of CuS-BSA/Lysozyme under Near Infrared Light Irradiation. Nanomaterials (Basel). Doi: 10.3390/nano11092156.

[56] C. Mutalik, R. Dwi and W. Hsu. (2022). Copper sulfide with morphology dependent photodynamic and photothermal antibacterial activities. Journal of Colloid and Interface Science. 607: 1825-1835.

[57] M. Saroja, M. Sathishkumar and M. Venkatachalam. (2019). Influence of (Cu, Al) doping concentration on the structural, optical and antimicrobial activity of ZnS thin films prepared by sol gel dip coating techniques. Optik. 182: 774-785.

[58] A. Menna, M. Amr and S. Mahrous. (2021). Preparation, Characterization, and Antibacterial Activity of ZnS-NP's Filled Polyvinylpyrrolidone/Chitosan Thin Films. Biointerface Research in Applied Chemistry. 11: 14336-14343.